

ISTS 2006-d-73\*

# OPTIMAL VARIABLE-SPECIFIC-IMPULSE RENDEZVOUS TRAJECTORIES BETWEEN HALO ORBITS

Michael Volle

a.i. solutions, Inc.

10001 Derekwood Lane, Ste. 215, Lanham, MD 20706, USA

(E-mail: michael.volle@ai-solutions.com)

## Abstract

Given the increasing number of missions that utilize Halo orbits, it is very likely that in the future there will be missions that use multiple spacecraft. With that idea in mind, this work considers the optimization of rendezvous trajectories for spacecraft starting on different Z-amplitude Halo orbits. An optimal control problem is derived that fixes the time-of-flight for the rendezvous trajectory, but allows the initial epoch to be free. The rendezvous trajectories are achieved using a finite burn, variable-specific-impulse engine where the thrust is varied according to a control law derived from optimal control theory. Several numerical examples are given to show the effects of various independent parameters, including time-of-flight, relative phasing of the two spacecraft, and the relative Z-amplitude of the Halo orbits.

## 1 Introduction

The problem of spacecraft rendezvous is well understood within the realm of two-body dynamics. However, the nature of the relative dynamics for two spacecraft is significantly different in the Circular Restricted Three Body Problem (CRTBP). Within two-body dynamics, orbits that are significantly different in size (semi-major axis) will have significantly different orbital periods, leading to a secular change in the relative phasing of the two spacecraft. Furthermore, the relative velocity of the two spacecraft will vary significantly, especially if the shape (eccentricity) of the orbits is different. These statements do not apply to Halo orbits of differing size (Z-amplitude). Increasing the Z-amplitude of Halo orbits does not significantly affect the period. For example, the sample halo orbits

shown in Fig. 1 both have an orbital period of approximately 180 days, and their synodic period is approximately 176 years. This indicates that while there is a secular change in the relative phasing of the spacecraft, it is much smaller, operating on the time scale of centuries, rather than weeks. Furthermore, the relative velocities experienced by the two spacecraft are significantly smaller. Whereas in two-body dynamics, relative velocities can be as high as kilometers per second, in the CRTBP, relative velocities are on the order of tens of meters per second. These differences in the relative periods, phasing, and velocities, significantly alters the nature of the rendezvous problem within the confines of the CRTBP.

In this study, the problem considered is that of optimizing the rendezvous of two spacecraft, each starting on Halo orbits of differing Z-amplitudes (or relative Z-amplitude) using a variable-specific-impulse (VSI) finite burn engine. The chaser spacecraft has a mass of 5000 kg, a maximum engine power of 500 W, and the propellant mass is specified to be 25% of the spacecraft mass. The solutions are generated by giving each spacecraft (target and chaser) an initial state at a reference epoch. The time-of-flight for the rendezvous trajectory is specified, and the initial epoch of the rendezvous trajectory is allowed to be free. The time of the actual rendezvous is then the initial epoch plus the time-of-flight. The controls to be optimized are the thrust direction, thrust magnitude, and power for the chaser spacecraft. The target spacecraft is assumed to be nominally coasting along its prescribed Halo orbit. Many different solutions were generated in an effort to analyze the effects of different independent parameters. The independent parameters considered in this work are: time-of-flight (TOF), relative Z-amplitude ( $\Delta Z_{amp}$ ) of the Halo orbits, and relative phasing ( $\Delta\phi$ ) of the target and chaser spacecraft.

There have been some previous works that are sim-

\*Copyright © 2006 by the Japan Society for Aeronautical and Space Sciences and ISTS. All Rights Reserved.

ilar to the analysis presented here. Senet, et al.[7], applied the same optimal control theory methodology to the problem of minimum time transfers from low Earth orbit to the invariant manifold of a Halo orbit using a VSI engine. Other works have considered the problem of optimizing transfers between Halo orbits through impulsive means, both in the CRTBP and in the Elliptic Restricted Three Body Problem. However, these works, by Hiday-Johnston, et al.[8, 9] and Simó, et al.[10] do not model a finite burn engine, and do not account for the timing constraints associated with the attempted rendezvous with another spacecraft.

The layout of the document is as follows. Section 2 discusses the dynamical model used in this analysis, how the Halo orbits were obtained, and the nature of the Halo orbits considered. Section 3 defines the optimal control problem and derives the transversality conditions associated with this problem. Section 4 contrasts two typical solutions in detail and also examines the trends associated with some independent parameters of the problem, such as time-of-flight, relative phasing of the two spacecraft, and relative Z-amplitude of the Halo orbits. Finally, in Section 5 some conclusions are made, and possible avenues of future study are identified.

## 2 Dynamical Model

### 2.1 Circular Restricted Three Body Equations

The dynamical model used in this study is that of the Circular Restricted Three Body Problem [1], with the Sun as one primary, and the Earth/Moon barycenter as the other. The Earth/Moon barycenter is assumed to orbit the Sun in a circular orbit. This system is normalized in mass, distance, and time, so that Newton's constant,  $G$ , is equal to unity. The equations for the normalization of the system are given in Eq. (1).

$$\begin{aligned} 1 \text{ MU} &= M_S + M_E + M_M \\ 1 \text{ DU} &= R_S - R_{E/M} \\ 1 \text{ TU} &= 2\pi \end{aligned} \quad (1)$$

The CRTBP is a well known dynamical model whose equations of motion [1] are  $[\ddot{x} = g_x, \ddot{y} = g_y, \ddot{z} = g_z]$  where

$$\mathbf{g} = \begin{bmatrix} 2\dot{y} + x - \frac{1-\mu}{r_1^3}(x+\mu) - \frac{\mu}{r_2^3}(x-1+\mu) \\ -2\dot{x} + y - \frac{1-\mu}{r_1^3}(y) - \frac{\mu}{r_2^3}(y) \\ -\frac{1-\mu}{r_1^3}(z) - \frac{\mu}{r_2^3}(z) \end{bmatrix} \quad (2)$$

where  $r_1$  and  $r_2$  are given by

$$r_1 = \sqrt{(x+\mu)^2 + y^2 + z^2} \quad (3)$$

$$r_2 = \sqrt{(x-1+\mu)^2 + y^2 + z^2} \quad (4)$$

and  $\mu$  is defined to be

$$\mu = \frac{M_E + M_M}{M_S + M_E + M_M}. \quad (5)$$

### 2.2 Determination of Halo Orbits

To obtain Halo orbits within the CRTBP, a common shooting method was applied [6]. Given an initial perpendicular crossing of the X-Z plane, the X coordinate, Y velocity and half the period are varied to achieve a second perpendicular crossing of the X-Z plane half an orbit later. The initial and final states are given below in Eq. (6)

$$\mathbf{X}_i = \begin{bmatrix} x = \text{guess}(1) \\ y = 0 \\ z = z_s \\ \dot{x} = 0 \\ \dot{y} = \text{guess}(2) \\ \dot{z} = 0 \end{bmatrix} \quad \mathbf{X}_f = \begin{bmatrix} x = \text{free} \\ y = 0 \\ z = \text{free} \\ \dot{x} = 0 \\ \dot{y} = \text{free} \\ \dot{z} = 0 \end{bmatrix}, \quad (6)$$

where  $z_s$  is the specified Z-amplitude of the desired Halo orbit and the final state,  $\mathbf{X}_f$ , is evaluated at  $t = \text{guess}(3)$ .

This method generates Halo orbits such as those seen in Fig. 1. The two Halo orbits shown repre-

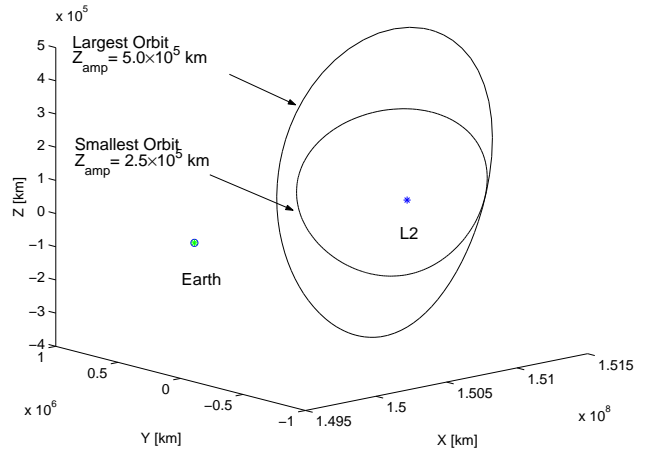


Figure 1:  $2.5 \times 10^5$  and  $5.0 \times 10^5$  km Halo Orbits

sent the largest and smallest Halo orbits considered in this work. The small Halo has a Z-amplitude of  $2.5 \times 10^5$  km and a period of 180.0774 days, while the large Halo has a Z-amplitude of  $5.0 \times 10^5$  km and a period of 179.5751 days. The synodic period of these two orbits was found to be 176.38 years. The value

of the Jacobi constant for the small Halo is 3.000809 and for the large Halo its value is 3.000761. Also, an additional product of the similar orbital periods is the fact that the orbital angular velocities are also very similar. Table 1 details these characteristics for all the Halo orbits considered in this analysis.

Table 1: Halo Orbit Characteristics

<b>Z-amp.</b> [km]	<b>Period</b> [days]	<b>Ang. Vel.</b> [°/day]	<b>Jacobi</b> <b>Constant</b>
$2.5 \times 10^5$	180.0774	1.999140	3.000809
$3.0 \times 10^5$	180.0065	1.999927	3.000801
$3.5 \times 10^5$	179.9215	2.000872	3.000793
$4.0 \times 10^5$	179.8218	2.001981	3.000784
$4.5 \times 10^5$	179.7067	2.003264	3.000773
$5.0 \times 10^5$	179.5751	2.004732	3.000761

## 3 Optimal Control Problem

### 3.1 State Equations and Spacecraft Controls

To set up the optimization problem, first the state and state dynamics must be defined:

$$\mathbf{X} = \begin{bmatrix} \mathbf{r} \\ \mathbf{v} \\ m \end{bmatrix} \quad (7)$$

and

$$\dot{\mathbf{X}} = \begin{bmatrix} \dot{\mathbf{r}} \\ \dot{\mathbf{v}} \\ \dot{m} \end{bmatrix} = \begin{bmatrix} \mathbf{v} \\ \mathbf{g}(\mathbf{r}, \mathbf{v}) + \frac{T}{m} \mathbf{u} \\ -\frac{T^2}{2P} \end{bmatrix} = \mathbf{f}(t, \mathbf{X}, \mathbf{u}), \quad (8)$$

where  $\mathbf{g}$  is the dynamical system defined by Eq. (2),  $T$  is the thrust magnitude,  $P$  is the engine power, and  $\mathbf{u}$  is the thrust direction unit vector. The control vector for the system is defined to be

$$\mathbf{u}_c = \begin{bmatrix} \mathbf{u} \\ T \\ P \end{bmatrix}. \quad (9)$$

When using a VSI engine, the thrust magnitude, thrust direction, and power are subject to the following constraints [7]

$$|\mathbf{u}| = 1 \quad (10)$$

$$0 \leq P \leq P_{max} \quad (11)$$

$$T = \frac{2P}{c} \quad (12)$$

where  $c$  is defined by

$$c = I_{sp} \cdot g_0 \quad (13)$$

and  $I_{sp}$  is the specific impulse of the engine and  $g_0 = 9.81$  m/s.

### 3.2 Cost Function and Optimal Controls

The performance index of the problem,  $J$ , is of the Mayer form and is defined to be

$$\max J = m_f. \quad (14)$$

With the inclusion of the boundary conditions and the problem Hamiltonian, the augmented performance index,  $J'$ , then becomes

$$\max J' = G + \int_{t_0}^{t_f} [H - \boldsymbol{\lambda}^T \dot{\mathbf{X}}] dt, \quad (15)$$

where  $\boldsymbol{\lambda}$  is a vector of co-states for the system,  $H$  is the problem Hamiltonian, and  $G$  is the end-point, or Bolza function. The Bolza function is the original performance index (Eq. (14)) with the boundary conditions of the problem adjoined using Lagrange multipliers, as shown below

$$G = m_f + \boldsymbol{\nu}_0^T \boldsymbol{\psi}_0 + \boldsymbol{\nu}_f^T \boldsymbol{\psi}_f, \quad (16)$$

where

$$\boldsymbol{\psi}_0 = \begin{bmatrix} \mathbf{r}_0 - \mathbf{r}_C(t_0) \\ \mathbf{v}_0 - \mathbf{v}_C(t_0) \end{bmatrix} = 0 \quad (17)$$

and

$$\boldsymbol{\psi}_f = \begin{bmatrix} \mathbf{r}_f - \mathbf{r}_T(t_f) \\ \mathbf{v}_f - \mathbf{v}_T(t_f) \end{bmatrix} = 0. \quad (18)$$

In Eqs. (17) and (18), the subscripts  $C$  and  $T$  indicate the chaser and target spacecraft, respectively. The problem Hamiltonian is defined to be

$$\begin{aligned} H &= \boldsymbol{\lambda}^T \mathbf{f} \\ &= \boldsymbol{\lambda}_r^T \mathbf{v} + \boldsymbol{\lambda}_v^T \left[ \mathbf{g}(\mathbf{r}, \mathbf{v}) + \frac{T}{m} \mathbf{u} \right] - \lambda_m \frac{T^2}{2P}. \end{aligned} \quad (19)$$

The augmented performance index (Eq. (15)) is then subject to the well known Euler-Lagrange conditions for optimality [4], which give the following relationships

$$\begin{aligned} \dot{\mathbf{X}} &= \mathbf{f} \\ \frac{\partial H}{\partial \mathbf{u}_c} &= \mathbf{0} \\ -\dot{\boldsymbol{\lambda}} &= \left( \frac{\partial H}{\partial \mathbf{X}} \right)^T \end{aligned} \quad (20)$$

Based on the final relationship in Eq. (20), the co-states of the system, given by  $\boldsymbol{\lambda} = [\boldsymbol{\lambda}_r, \boldsymbol{\lambda}_v, \lambda_m]^\top$ , are also subject to their own equations of motion. These are given by

$$\dot{\boldsymbol{\lambda}} = - \left( \frac{\partial H}{\partial \mathbf{X}} \right)^\top = \begin{bmatrix} -\boldsymbol{\lambda}_v^\top \left( \frac{\partial \mathbf{g}}{\partial \mathbf{r}} \right) \\ -\boldsymbol{\lambda}_r - \boldsymbol{\lambda}_v^\top \left( \frac{\partial \mathbf{g}}{\partial \mathbf{v}} \right) \\ \boldsymbol{\lambda}_v^\top \mathbf{u} \left( \frac{T}{m^2} \right) \end{bmatrix}. \quad (21)$$

Taking the derivative of the Hamiltonian with respect to the control vector  $\mathbf{u}_c$  maximizes the Hamiltonian, and yields the optimal controls for the rendezvous trajectories [2, 3]. The derivatives of the Hamiltonian with respect to  $\mathbf{u}$  and  $T$  yield

$$\begin{aligned} \mathbf{u} &= \frac{\boldsymbol{\lambda}_v}{\lambda_v} \\ T &= \frac{\lambda_v P_{max}}{\lambda_m m} \end{aligned} \quad (22)$$

Using the first relationship in Eq. (22), the derivative of the mass co-state can be rewritten as

$$\dot{\lambda}_m = \lambda_v \frac{T}{m^2}. \quad (23)$$

and the Hamiltonian can be rewritten as

$$H = \boldsymbol{\lambda}_r^\top \mathbf{v} + \boldsymbol{\lambda}_v^\top \mathbf{g}(\mathbf{r}, \mathbf{v}) + S \cdot T \quad (24)$$

where the Switching Function,  $S$ , is defined to be

$$S = \frac{\lambda_v}{m} - \frac{T}{2P} \lambda_m. \quad (25)$$

The derivative of the Hamiltonian with respect to  $P$  indicates that when the mass co-state ( $\lambda_m$ ) is positive,  $P = P_{max}$ , and since  $\lambda_m$  will have a positive initial value (See Section 3.4) and its derivative is positive (Eq. (23)), the spacecraft will always operate at maximum power. Finally, since the spacecraft will always be at maximum power and the thrust must always be positive, this indicates that the Switching Function (Eq. (25)) will always be positive.

### 3.3 Transversality Conditions

Now the transversality conditions at the boundaries must be considered. When using a VSI engine, the time-free problem when  $t_0$  and  $t_f$  are both free, is not possible due to the nature of the VSI engine[7]. In the time-free formulation, thrust,  $t_0$ , and  $t_f$  can all be varied, and this makes it possible to drive the

solution to a nearly infinite time-of-flight and an infinitesimal thrust. To avoid this situation, some form of constraint must be placed on the time-of-flight. For this analysis, the time-of-flight was specified, and  $t_0$  was allowed to be free, e.g.

$$t_f = t_0 + TOF_s. \quad (26)$$

Based on the first differential of the augmented performance index, the following relationships define the transversality conditions for the free initial time problem with a fixed time-of-flight

$$- \frac{\partial \mathbf{G}}{\partial \mathbf{X}_0} = \boldsymbol{\lambda}_0 \quad (27)$$

$$\frac{\partial \mathbf{G}}{\partial \mathbf{X}_f} = \boldsymbol{\lambda}_f \quad (28)$$

$$\frac{\partial \mathbf{G}}{\partial \mathbf{t}_0} + \frac{\partial \mathbf{G}}{\partial \mathbf{t}_f} = H|_{t_0} - H|_{t_f}. \quad (29)$$

However, provided the gravitational force,  $\mathbf{g}$ , is not a function of time, the First Integral exists, and therefore the Hamiltonian remains constant [4]. Within the CRTBP, the First Integral does exist ( $\dot{H} = 0$ ), so the following equality applies

$$H|_{t_0} = H|_{t_f} \quad (30)$$

and Eq. (29) can be rewritten as

$$\frac{\partial \mathbf{G}}{\partial \mathbf{t}_0} = - \frac{\partial \mathbf{G}}{\partial \mathbf{t}_f}. \quad (31)$$

The partial derivatives in Eqs. (27) and (28) are shown below

$$- \frac{\partial \mathbf{G}}{\partial \mathbf{X}_0} = \begin{bmatrix} -\boldsymbol{\nu}_{r_0} \\ -\boldsymbol{\nu}_{v_0} \\ -\boldsymbol{\nu}_{m_0} \end{bmatrix} = \begin{bmatrix} \boldsymbol{\lambda}_{r_0} \\ \boldsymbol{\lambda}_{v_0} \\ \boldsymbol{\lambda}_{m_0} \end{bmatrix} \quad (32)$$

$$\frac{\partial \mathbf{G}}{\partial \mathbf{X}_f} = \begin{bmatrix} \boldsymbol{\nu}_{r_f} \\ \boldsymbol{\nu}_{v_f} \\ 1 \end{bmatrix} = \begin{bmatrix} \boldsymbol{\lambda}_{r_f} \\ \boldsymbol{\lambda}_{v_f} \\ \boldsymbol{\lambda}_{m_f} \end{bmatrix}. \quad (33)$$

This information can then be combined with the derivatives of the Bolza function with respect to the initial and final times, shown below

$$\frac{\partial \mathbf{G}}{\partial \mathbf{t}_0} = \boldsymbol{\nu}_{r_0}^\top \mathbf{v}_{C_0} + \boldsymbol{\nu}_{v_0}^\top \mathbf{g}_{C_0} \quad (34)$$

$$\frac{\partial \mathbf{G}}{\partial \mathbf{t}_f} = \boldsymbol{\nu}_{r_0}^\top \mathbf{v}_{T_f} + \boldsymbol{\nu}_{v_f}^\top \mathbf{g}_{T_f} \quad (35)$$

where the subscripts  $C_0/T_0$  and  $C_f/T_f$  represent the chaser/target spacecraft at the initial and final times,

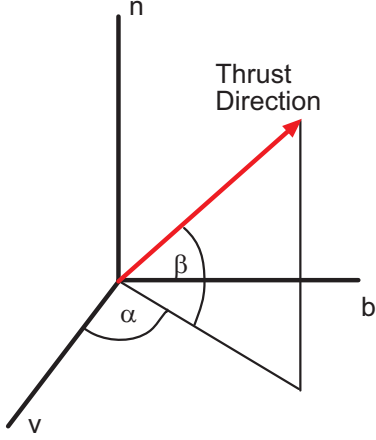


Figure 2: Thrust Direction in Vehicle-Centered Frame

respectively. The combinations of Eq. (32) with Eq. (34) and Eq. (33) with Eq. (35) means that Eq. (31) can be rewritten as

$$\lambda_{r_0}^T \mathbf{v}_0 + \lambda_{v_0}^T \mathbf{g}_0 = \lambda_{r_0}^T \mathbf{v}_f + \lambda_{v_f}^T \mathbf{g}_f \quad (36)$$

and this can be used as the required transversality condition for the optimal control problem. However, since each side of Eq. (36) is equal to the Hamiltonian without the product of the Switching Function times the thrust, an equivalent condition is

$$S_0 \cdot T_0 = S_f \cdot T_f. \quad (37)$$

Either Eq. (36) or Eq. (37) can be used in the boundary value problem that will be defined in Section 3.5. The condition that will be used in this analysis is Eq. (37).

### 3.4 Adjoint Control Transformation

To combat the difficulty of guessing the initial co-states, the Adjoint Control Transformation (ACT) was developed by Dixon, et al. [5]. The transformation relates the initial co-states to the thrust direction, as described by two spherical angles in a vehicle centered frame. In this analysis, consider a velocity reference frame with the unit vectors of this frame defined as

$$\hat{\mathbf{v}} \equiv \frac{\mathbf{v}}{v} \quad \hat{\mathbf{b}} \equiv \hat{\mathbf{n}} \times \hat{\mathbf{v}} \quad \hat{\mathbf{n}} \equiv \frac{\mathbf{r} \times \mathbf{v}}{|\mathbf{r} \times \mathbf{v}|}. \quad (38)$$

Within this frame, the thrust direction and its derivative are determined from two spherical angles,  $\alpha$  and  $\beta$ , and their derivatives. A graphical representation is shown in Fig. 2. The equation for the thrust direction

in terms of the spherical angles is

$$\hat{\mathbf{u}}_{vbn} = \begin{pmatrix} \cos(\alpha) \cdot \cos(\beta) \\ \sin(\alpha) \cdot \cos(\beta) \\ \sin(\beta) \end{pmatrix} \quad (39)$$

and its derivative is

$$\dot{\hat{\mathbf{u}}}_{vbn} = \begin{pmatrix} -\dot{\alpha} \sin(\alpha) \cdot \cos(\beta) - \dot{\beta} \cos(\alpha) \cdot \sin(\beta) \\ \dot{\alpha} \cos(\alpha) \cdot \cos(\beta) - \dot{\beta} \sin(\alpha) \cdot \sin(\beta) \\ \dot{\beta} \cos(\beta) \end{pmatrix}. \quad (40)$$

However, to properly obtain the co-states, the thrust direction is needed in the frame in which the vehicle is integrated. This requires a rotation matrix, defined to be

$$\mathbf{R} = \begin{pmatrix} \hat{\mathbf{x}} \cdot \hat{\mathbf{v}} & \hat{\mathbf{x}} \cdot \hat{\mathbf{b}} & \hat{\mathbf{x}} \cdot \hat{\mathbf{n}} \\ \hat{\mathbf{y}} \cdot \hat{\mathbf{v}} & \hat{\mathbf{y}} \cdot \hat{\mathbf{b}} & \hat{\mathbf{y}} \cdot \hat{\mathbf{n}} \\ \hat{\mathbf{z}} \cdot \hat{\mathbf{v}} & \hat{\mathbf{z}} \cdot \hat{\mathbf{b}} & \hat{\mathbf{z}} \cdot \hat{\mathbf{n}} \end{pmatrix} \quad (41)$$

and it is used below

$$\hat{\mathbf{u}}_{xyz} = \mathbf{R} \hat{\mathbf{u}}_{vbn}. \quad (42)$$

Rotating  $\dot{\hat{\mathbf{u}}}$  is also achieved through a similar transformation.

$$\dot{\hat{\mathbf{u}}}_{xyz} = \dot{\mathbf{R}} \hat{\mathbf{u}}_{vbn} + \mathbf{R} \dot{\hat{\mathbf{u}}}_{vbn}. \quad (43)$$

By re-arranging the definition of the primer vector (Eq. (22)) the following equation is obtained:

$$\lambda_v = \lambda_v \hat{\mathbf{u}}_{xyz}. \quad (44)$$

Then, by taking the derivative of Eq. (44), the following is obtained

$$\dot{\lambda}_v = \dot{\lambda}_v \hat{\mathbf{u}}_{xyz} + \lambda_v \dot{\hat{\mathbf{u}}}_{xyz}. \quad (45)$$

This equation can then be combined with the equation of motion for  $\lambda_r$  in Eq. (21) to obtain the equation for the initial values of  $\lambda_r$ , which is

$$\lambda_r = -\dot{\lambda}_v \hat{\mathbf{u}}_{xyz} - \lambda_v \dot{\hat{\mathbf{u}}}_{xyz}. \quad (46)$$

Using Eqs. (46) and (44), the initial values of the co-states can be determined from the spherical angles of the primer vector in the vehicle-centered frame.

This process assumes the initial mass co-state ( $\lambda_m$ ) to be unity and removes the constraint on the final mass co-state. As found in Eq. (33), the final mass co-state is unity, and from Eq. (23), its derivative is always positive, so the final value will be greater than one. Setting the initial mass co-state to unity simply scales the mass multiplier by its final value. Since the optimization problem considered is

$$\max J = m_f, \quad (47)$$

the ACT rescales the problem as such

$$\max J = K \cdot m_f, \quad (48)$$

where K is some positive arbitrary constant.

### 3.5 The Boundary Value Problem

Based on the development of the previous sections, the boundary value problem can now be formed. The FORTRAN non-linear equation solving package, NS11AD, provided from the archive of the Harwell Subroutine Library [11], was used to solve the boundary value problem. The NS11AD uses a combination of Newton's method and steepest descent, and estimates the Jacobian matrix based on numerical derivatives. The vector of initial guesses for the boundary value problem is given below

$$\mathbf{z}_g = \begin{bmatrix} \alpha_0 \\ \beta_0 \\ \dot{\alpha}_0 \\ \dot{\beta}_0 \\ \lambda_{v0} \\ \dot{\lambda}_{v0} \\ t_0 \end{bmatrix} \quad (7x1) \quad (49)$$

Next, the vector of constraints for the problem is provided. When these constraint functions are evaluated to be less than a specified convergence tolerance, the solution is deemed to be optimal.

$$\mathbf{z}_c = \begin{bmatrix} \mathbf{r}_f - \mathbf{r}_{Tf} \\ \mathbf{v}_f - \mathbf{v}_{Tf} \\ S_0 \cdot T_0 - S_f \cdot T_f \end{bmatrix} \quad (7x1) \quad (50)$$

## 4 Numerical Examples

In this section, numerical results of this analysis are presented. First, the boundary value problem is validated numerically by comparing time-fixed solutions to the free initial time solutions. Secondly, two example solutions are contrasted, with the prescribed TOF being 70 and 90 days. These examples represent the two types of optimal solutions obtained in this analysis. Finally, results are presented that indicate the behavior of the solution space when independent parameters are varied.

### 4.1 Validation of Boundary Value Problem

Before the results are presented, the validation of the transversality conditions should be considered. To characterize the behavior of the boundary value problem, the free initial time solution was compared to a series of time-fixed solutions, all having the same specified TOF. The optimal free initial time solution should correspond to a local minimum in the series of time fixed solutions. For a time fixed solution using a VSI

engine, there are no transversality conditions at the initial or final times, therefore the chaser spacecraft must simply match the target's position and velocity at the final time.

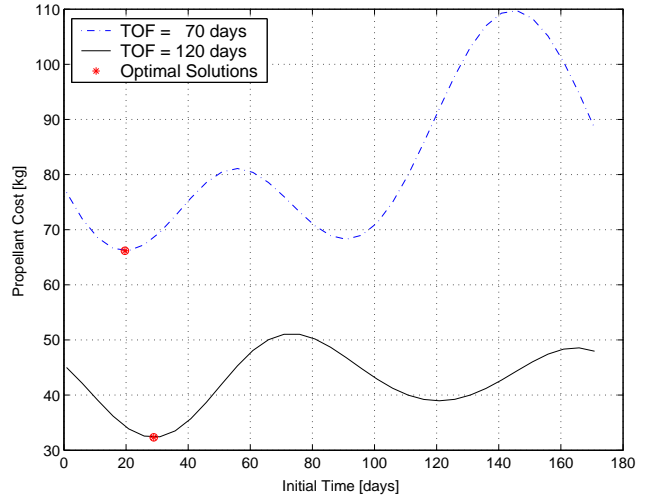


Figure 3: Validation of the Free Initial Time Solutions

Fig. 3 shows the propellant consumption for a series of time fixed solutions using two different values for time-of-flight. The two values for TOF are 70 and 120 days. The series of solutions has initial times in the range of 0 to 180 days, or roughly one orbit. Since the change in the relative phasing is very small, the pattern of propellant consumption should remain roughly constant for several orbits. It can be seen that both sets of solutions have two local minima. For each time-of-flight, a free initial time solution was also calculated, and these solutions are indicated by the red asterisks. It can be seen that the free initial time solutions are located at the local minima. This indicates that the transversality conditions were derived properly, and the boundary value problem is behaving as it should.

### 4.2 Seventy & Ninety Day Time-of-Flight Cases

In order to contrast the two basic types of solutions obtained in this analysis, two solutions with TOF = 70 and TOF = 90 days are considered. It was found that with a TOF of less than about 83 days, the optimal solutions occurred near the maximum -Y excursion of the Halo orbits. For solutions with a TOF of greater than 83 days, the optimal solutions occurred near the maximum -Z excursion.

In Figs. 4-6, the plots in the left column correspond to the 70 day time-of-flight case and the right hand column is the 90 day time-of-flight. The optimal rendezvous trajectories for these two cases are shown

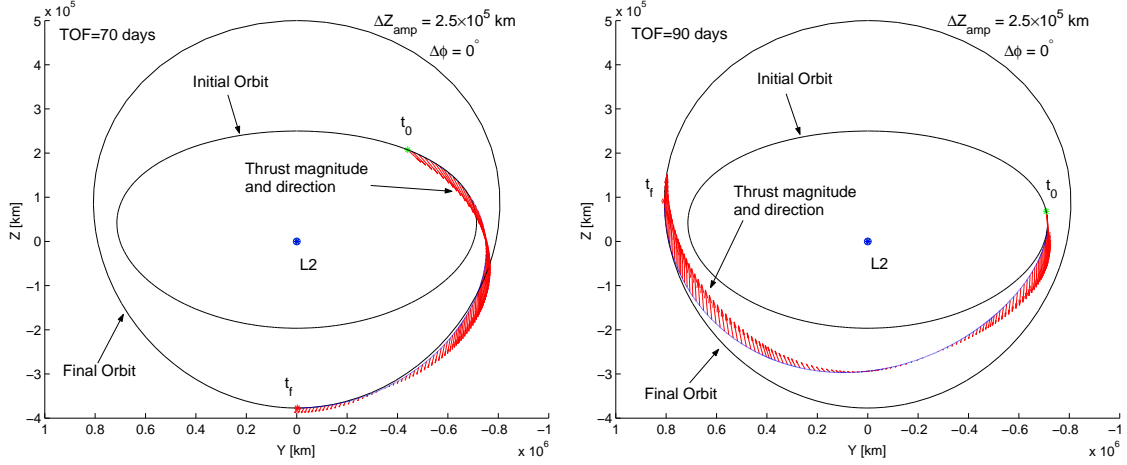


Figure 4: Optimal Seventy & Ninety Day Trajectories

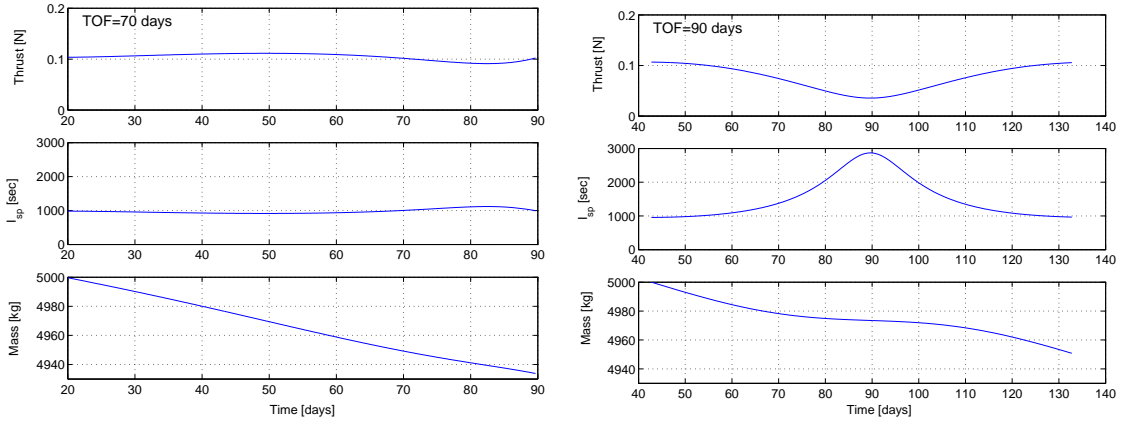


Figure 5: Optimal Engine Performance for Seventy & Ninety Day Trajectories

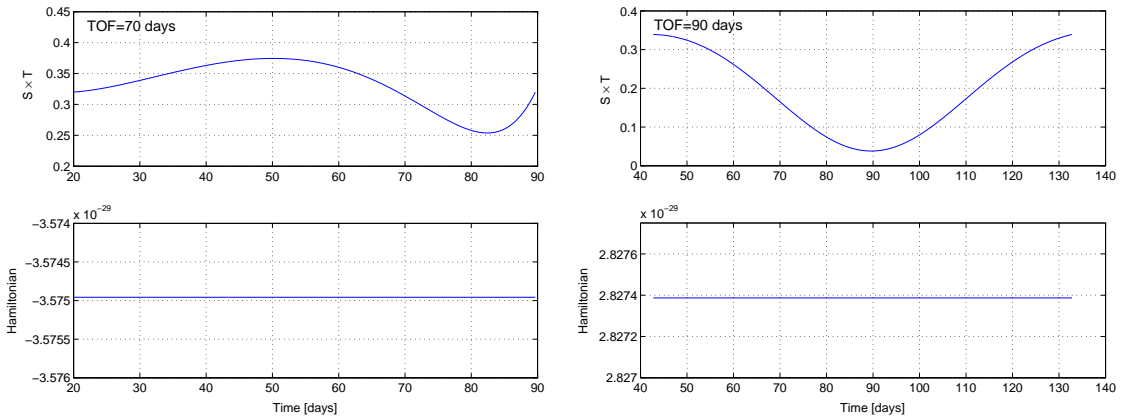


Figure 6: Parameters of the Optimization Problem for Seventy & Ninety Day Trajectories

in Fig. 4. The view of the plots is along the Sun-Earth/Moon line, looking out towards L2. The red arrows indicate the magnitude and direction of the thrust over the course of the trajectories. It can be seen that these two trajectories illustrate the differences in location of the two different types of solutions

obtained in this analysis.

Additionally, it can be seen from the plots in Fig. 5 that the performance of the VSI engine in each case is considerably different as well. The engine performance of the 70 day solution is nearly constant, with both the thrust and specific impulse only varying by

approximately 10%. On the other hand, the 90 day solution exhibits what is nearly a thrust-coast-thrust structure. Near the midpoint of the trajectory, the thrust is reduced by nearly 70% and the specific impulse increases by nearly 200%. It can also be seen that the propellant cost in the 90 day case is less than that in the 70 day case.

Finally, the transversality conditions of the problem must be considered. Eq. (50) stated that the product of the Switching Function and Thrust should be equal at the initial and final times. Also, Eq. (30), which states the Hamiltonian is constant, was used to obtain this condition on the Switching Function, so therefore both conditions must be satisfied numerically to have a valid solution. From the plots in Fig. 6, it can be seen that both these requirements are met for both the 70 and 90 day solutions.

### 4.3 Analysis of Independent Parameters

Now that the characteristics of two example optimal solutions have been examined, the characteristics of the solution space will be considered. There are several independent parameters that can be used to characterize the solution space. The parameters considered in this analysis are TOF,  $\Delta\phi$ , and finally  $\Delta Z_{amp}$  of the Halo orbits.

First, consider the effect of the rendezvous trajectory time-of-flight. Section 4.2 showed that there are two distinct types of optimal solutions at different values of TOF. To avoid comparing the two different types of solutions here, time fixed cases were run. With  $\Delta Z_{amp}$  fixed, and the relative phasing angle at  $\Delta\phi = 0^\circ$ , several cases were run, varying the TOF by 10 days, with values in the range of 30 to 120 days. The results are shown below in Fig. 7, and they are of the form that one would expect. The cost of the rendezvous is shown both in propellant cost as well as  $\Delta V$ . The shorter the time-of-flight, the greater the propellant (or  $\Delta V$ ) cost. It can also be seen that there is a point of diminishing returns where significant increases in the time-of-flight do not save much in terms of propellant or  $\Delta V$ .

Next consider the effect of the relative phasing of the two spacecraft. For a given time-of-flight and relative Z-amplitude separation, in this case TOF = 120 days and  $\Delta Z_{amp} = 2.5 \times 10^5$  km, several cases were run with the relative phasing angle ranging from  $\Delta\phi = -55^\circ$  to  $55^\circ$ . A negative phasing angle indicates that the chaser spacecraft is trailing the target spacecraft, and a positive angle indicates the chaser is leading the target. Fig. 8 shows both the optimal propellant consumption and  $\Delta V$  for the various relative phasing an-

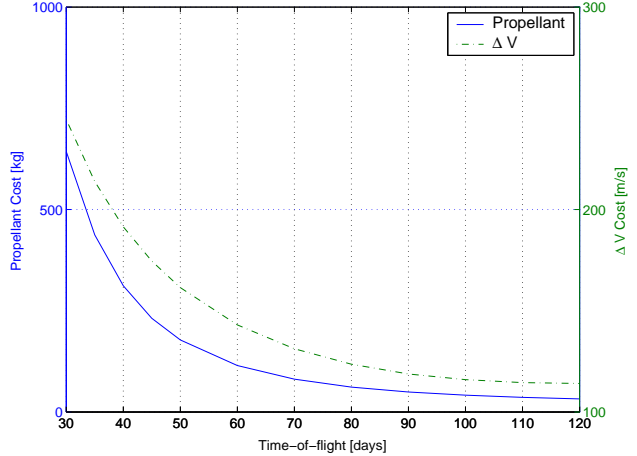


Figure 7: Propellant &  $\Delta V$  Cost vs. Time-of-Flight

gles. For this case, the optimal phasing is right around  $\Delta\phi = 1^\circ$ , which makes sense when considering the relative periods of the two Halos. As stated previously, the synodic period of these two Halos is 176.38 years, which indicates the change in the relative phasing is about  $1^\circ$  per orbit. Since the target spacecraft on the  $5.0 \times 10^5$  km Halo orbit has a slightly shorter period, it will advance ahead of the chaser spacecraft at about  $1^\circ$  per orbit. Therefore, the optimal occurs when the chaser spacecraft is leading in terms of phase angle, by an amount roughly equal to the rate of advance of the target.

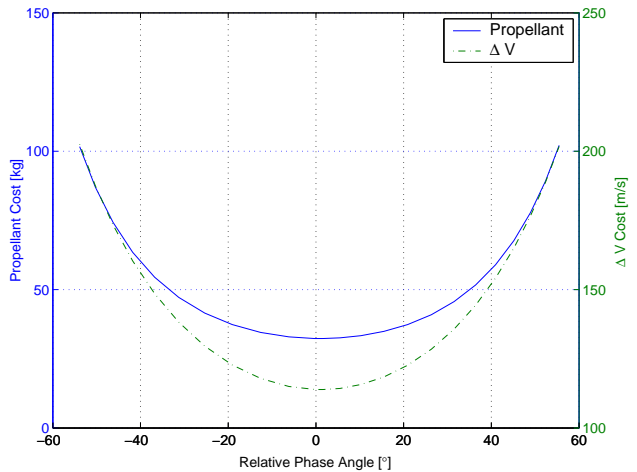


Figure 8: Propellant &  $\Delta V$  Cost vs. Relative Phasing Angle

Additionally, it can be seen that at a relative phase angle of  $\Delta\phi = \pm 55^\circ$ , the propellant consumption rises to a value that is roughly triple the value at the optimal relative phase angle. This is due to the chaser spacecraft either catching up to the target, or allowing the target to make up the difference. The two plots

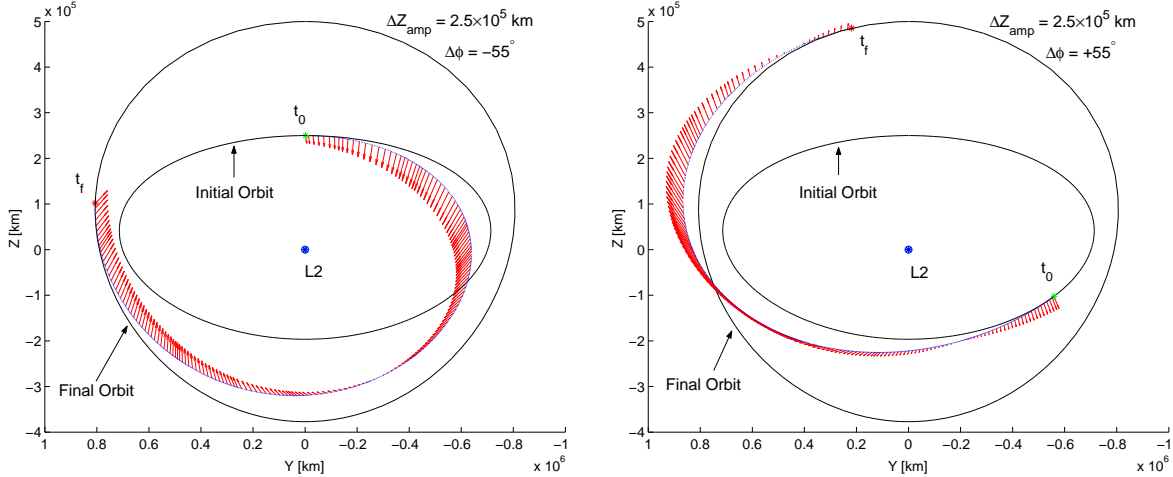


Figure 9: Trajectories Showing Compensation for Differences in Relative Phase Angle

in Fig. 9 illustrate how this is done. The plot on the left shows how the chaser spacecraft goes within the initial Halo orbit to catch up to the target when the chaser is lagging behind in phase angle. The plot on the right shows how the chaser moves out beyond the target's orbit to allow the target spacecraft to catch up. Since all the orbits have very similar orbital angular velocities (see Table 1), it will be impossible to use an intermediate orbit to compensate for phase angle differences, similar to the use of a phasing loop for lunar trajectories.

To consider the effect of  $\Delta Z_{amp}$  on the propellant consumption, a series of free initial time solutions was generated for trajectories between the Halo orbits listed in Table 1. The results of this analysis are shown in Fig. 10. It can be seen that there is almost a linear relationship between the relative Z-amplitude and the  $\Delta V$  cost. This proportionality is in agreement with the results presented by Simó et al. [10].

## 5 Conclusions

There are some distinct differences in the rendezvous problem when switching from the two-body dynamical system to the CRTBP. The relative nature of the chaser and target spacecraft orbits represents several of those differences. The large synodic period of Halo orbits of differing Z-amplitudes leads to windows that last for years in which rendezvous trajectories are possible. Also, the small relative velocities of the orbits allows for a large range of relative phasings for the two spacecraft. The small relative velocities can also make it possible for the chaser spacecraft to have a nearly constant thrust profile over the course of the rendezvous trajectory.

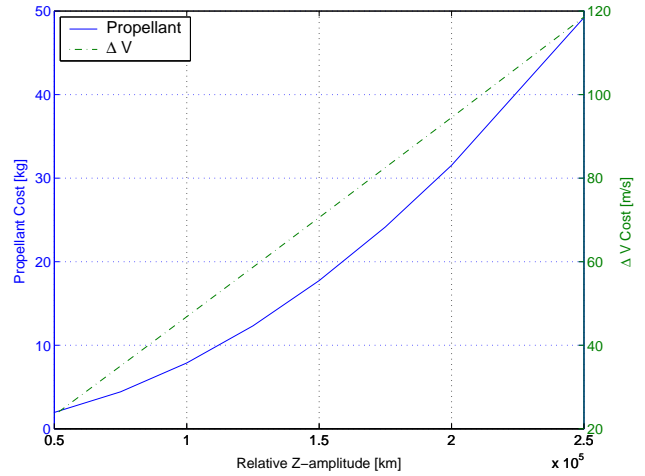


Figure 10: Propellant &  $\Delta V$  Cost vs. Relative Z-amplitude

There are several conclusions that have been made based on this analysis, and they are listed below.

- When using a VSI engine, there are many possible rendezvous trajectories between Halo orbits.
- Rendezvous trajectories are possible for a wide range of relative phasings, with a relative phasing of about  $1^\circ$  being the optimal phasing for the cases studied.
- Due to the similar orbital angular velocities, it is not possible to use an intermediate orbit to correct relative phase differences between spacecraft.
- There is a nearly linear relationship between relative Z-amplitude and  $\Delta V$  cost.
- In both types of solutions, as the time-of-flight

increases, change in the optimal thrust profile decreases until it is nearly constant.

Based on the results of the analysis presented here, the following future avenues of study will be considered.

- Analysis of the rendezvous problem using a constant-specific-impulse (CSI) engine where thrust magnitude is no longer a control to be optimized.
- Perform a higher fidelity analysis using an ephemeris based system.

## Acknowledgments

The analysis presented here was supported, both financially and otherwise, by Robert Sperling and Conrad Schiff of a.i. solutions, Inc.

## References

- [1] V. Szebehely. *Theory of Orbits: The Restricted Problem of Three Bodies*, Academic Press, New York, 1967.
- [2] L. S. Pontryagin, V. G. Boltyanskii, R. V. Gamkrelidze, and E. F. Mischchenko. *The Mathematical Theory of Optimal Processes*, Wiley-Interscience, New York, 1963.
- [3] D. E. Lawden, *Optimal Trajectories for Space Navigation*, Butterworths, London, 1963.
- [4] David Hull, *Optimal Control Theory for Applications*, Springer-Verlag, New York, 2003.
- [5] L. C. Dixon and M. C. Bartholomew-Biggs. “Adjoint Control Transformations for Solving Practical Optimal Control Problems,” *Optimal Control Applications and Methods*, Vol. 2, pp. 365-381, 1981.
- [6] D. L. Richardson. “Analytic Construction of Periodic Orbits about the Collinear Points,” *Celestial Mechanics*, Vol. 22, No. 3, pp. 241-253, 1980.
- [7] Juan Senent, Cesar Ocampo and Antonio Capella. “Low-Thrust Variable-Specific-Impulse Transfers and Guidance to Unstable Periodic Orbits,” *Journal of Guidance, Control, and Dynamics*, Vol. 28, No. 2, March-April 2005, pp. 280-290.
- [8] K. C. Howell and L. A. Hiday-Johnston. “Time-Free Transfers Between Libration-Point Orbits in the Elliptic Restricted Problem,” *Acta Astronautica*, Vol. 32, No. 4, 1994, pp. 245-254.
- [9] L. A. Hiday and K. C. Howell. “Impulsive Time-Free Transfers Between Halo Orbits,” *AIAA/AAS Astrodynamics Conference*, Hilton Head, S.C. 1992.
- [10] G. Gómez, A. Jorba, C. Simó. “Study of the Transfer Between Halo Orbits,” *Acta Astronautica*, Vol. 43, No. 9-10, pp. 493-520, 1998.
- [11] “Archives of the Harwell Subroutine Library,” AEA Technology, Harwell Lab., Oxfordshire, England, U.K., Dec. 1995.